THERMOLUMINESCENCE AND OPTICAL PROPERTIES OF Dy^{3+} DOPED MgO NANOPARTICLES, PREPARED BY SOLUTION COMBUSTION SYNTHESIS METHOD

GITANJALI SAHU[a1], ANUBHA S. GOUR[b] AND RAJU KUMAR CHANDRAKAR[c]

[ab]SOS in Physics and Astrophysics, Pt. Ravishankar Shukla University, Raipur, Chhattisgarh, India
[c]Department of Physics, National Institute Raipur, Chhattisgarh, India

ABSRACT

The present paper reports that the thermoluminescence and optical properties of Dy^{3+} doped MgO nanoparticles, prepared the Solution Combustion Synthesis (SCS) method. MgO:Dy^{3+} samples were characterized by powder X-ray diffraction analysis (XRD), infrared (FTIR) spectroscopy, scanning electron microscopy (SEM) and high resolution transmission electron microscope (HRTEM). The thermoluminescence (TL) glow curve was recorded by heating the sample exposed to UV-radiation, at a fixed heating rate 1°C sec^{-1}. In view of this, we have prepared small size of nanoparticles with different concentration of Dy^{3+} doped MgO nanoparticles. The TL glow curve of MgO:Dy^{3+}, they have a simple structure with two prominent peak, one peak around 152 ^{0}C and second peak around 250 ^{0}C, moreover, the both peak does not shift towards to the shorter temperature, but intensity of glow peak increases with increasing dopant concentration of Dy^{3+} and was observe. The activation energy of the samples was in the range for peak-I 0.46 eV to 0.42 eV and for peak-II 1.33 eV to .90 eV the order of frequency factor of the samples was found in the range for peak-I 1.01×10^{17} s^{-1} to 0.65×10^{16} s^{-1} and for peak-II 5.78×10^{28} s^{-1} and 2.78×10^{28} s^{-1} and the TL follows second order kinetics.

KEYWORDS: Thermoluminescence, Nanoparticles, MgO:Dy^{3+}.

When an insulator or semiconductor previously exposed to ionizing radiation such as X-rays, γ-rays, β-particles or α-particles or any other radiations is heated, then the energy stored in the phosphors, as a result of irradiation process, liberates in the form of visible light in addition to the normal thermal radiation. The additional visible light emitted during first heating is called thermally stimulated luminescence (TSL) or simply thermoluminescence (TL).

Reheating such phosphors cooled to room temperature gives rise to only normal thermal emission, in which additional non-thermal visible light is not emitted. When an irradiated coloured crystal is heated at a rapid rate, holes or electrons are set free from the traps (defect sites) and emission takes place when they recombine with a charge of opposite sign. The defect sites which release the carriers are known as traps. In contrast, the centres from where thermal releases of carriers, etc. are not possible, but where the probability of capture of charges of opposite sign is appreciable, are called recombination centres. Presently the thermoluminescence continues to be an active area of research because of its immense contribution in the field of personnel and environmental dosimetry, dating of archaeological artifacts, sediments and study of defects in solids, etc.[1-6]

Over the past few years many advances have been made in the area of preparation of nanomaterials. Nanotechnology has made nanocrystalline materials become an area of intense research activity [7–10]. Nanocrystalline materials are polycrystal- line materials with grain size below 100 nm [11, 12]. The change in the crystalline size and shape will alter the properties, which were formerly thought to be constant for a given material. Nanocrystals of common metal oxides have been shown to be highly efficient and active adsorbents for many toxic chemicals, including air pollutants, and chemical warfare agents [13]. Magnesium oxide (MgO), as an exceptionally important material for using in catalysis [14,15], toxic waste remediation, or as additives in refractory, paint, and superconductor products [16] has been attracting both fundamental and application studies [17]. Many different synthetic routes provide nanoscale MgO including sol–gel [18], hydrothermal/solvothermal [19,20], laser vaporization [21], chemical gas phase deposition [22], aqueous wet chemical [23], surfactant methods [24], polyol-mediated thermolysis process [25], and microwave-assisted method [26]. In recent years metal and semiconductor received considerable attention as active components in wide variety of research and technological application due to their optical, electric and magnetic properties compare to the bulk modular parts[27-29].Magnesium oxide is an interesting basic oxide that has many application in catalysis, absorption and synthesis of refectory ceramics [30-33]. MgO is a wide band gap insulator (7.8ev) with rock salt crystal structure (fcc) at ambient pressure, the Mg ions occupying octahydral sites in anion closed packed structure ([34,35]. Dy 3+ ions are well known activator dopants for many different inorganic lattice producing white light emission by suitably adjusting yellow and blue emission [36]. Although the PL such as

[1]Corresponding author

borate, niobate and phosphate has drawn attention[37,38]. MgO:Dy3+ has commonly being prepared using combustion syntheses method at temperature of 550° C. This method is one of the best method because it is relatively simple, efficient, low cost and time consuming method. The scope of this work is to analyze crystalline nature, spectrum and atomic percentage of sample. The present results prove that the combustion technique using MgO:Dy^{3+} can produce the materials with high crystallinity. The results in this study show that the SCS technique can potentially produce materials with TL intensity comparable to commercial dosimetric materials, although further optimizations are still required.

EXPERIMENTAL

The starting raw materials are magnesium nitrate [$Mg(NO_3)_2.6H_2O$] urea [NH^2CONH^2] and dysprosium nitrate. These raw materials were firstly weighted first and were taken in mortar pistal and mixed it properly for one hour. After mixing, these materials are placed in crucible was then introduced into muffle furnace at 550°C for 20 min as the ignition occurs the reaction occurs vigorously for few seconds and the fluffy substance was obtained. Based on mass ratio of the experiment the overall reaction equation could be expressed as follows:

$$6[Mg(NO_3)_2.6H_2O]+6[Dy(NO_3)_3.6H_2O]+28[NH_2CONH_2] = 6MgO:Dy+43N_2+28CO_2$$

The morphologies and sizes of the mercaptoethanol capped MgO: Dy3+ nanoparticles were determined by X-ray diffraction(XRD) studies with Cu Kα radiation (λ=1.5418Å). XRD data were collected over the range 20-70^0 at room temperature. X-ray diffraction patterns were obtained using a Rigaku Rotating Anode (H-3R) diffractometer. In XRD the particle size was calculated using the Debye-Scherrer formula. The particle size was also calculated using the field emission gun scanning electron microscope (FEGSEM) and high resolution transmission electron microscope (HRTEM) methods. The thermoluminescence was recorded with the help of a TLD reader in which the heating rate was 1^{0}C/s. The model of TLD reader is TL 1009I and its make is NUCLEONIX.

RESULTS AND DISSCUSSION

X-Ray Diffraction (XRD) Study

The XRD patterns for the samples are shown in Fig. 3.1 MgO:Dy^{3+} nanocrystals for four different concentrations (Dysprosium), Three different peaks are obtained at 2θ values of 32.36, 42.65 and 62.34. This shows that the samples have cubic structure and the peaks correspond to diffraction at (111), (200) and (220) planes, respectively. The lattice parameter has been computed as 5.31Å, which is very close to the standard value (5.42Å). It is also seen from Fig. 3.1 that peaks intensity are increases for higher concentration of dopent. The size of the particle has been computed from the width of the first peak using Debye-Scherrer formula (39) given below:

$$D=\frac{K\lambda}{\beta\cos\theta} \qquad \ldots(3.1)$$

where K is constant (K=0.9), λ the wavelength of X-ray, β the full width at half maximum and θ is Bragg angle. The particle sizes obtained from XRD were in the range 1 nm - 3 nm.

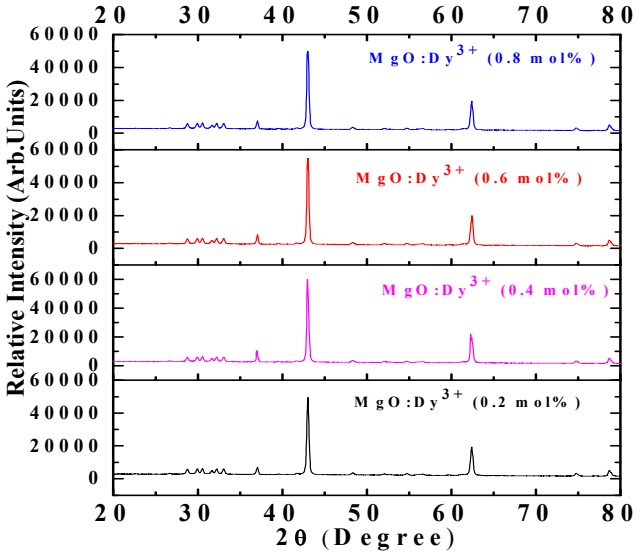

Figure 1: XRD pattern of MgO nanocrystals of different concentration of Dy^{3+}.

EDX (Energy Dispersive X-ray)

Fig.2a shows the spectrum obtained by EDX samples is shown in Fig.2b from the sample spectrum 100% of Mg metal was observed in the sample corresponding to peak shown in the Fig3b. In sample the inclusion of Dy^{3+} is shown in thes corresponding peaks. From the data it is observed that the synthesized sample contains about Mg, O and Dy with 55.71%, 44.32% and 0.87% of atomic percentage respectively which agrees with expected value.

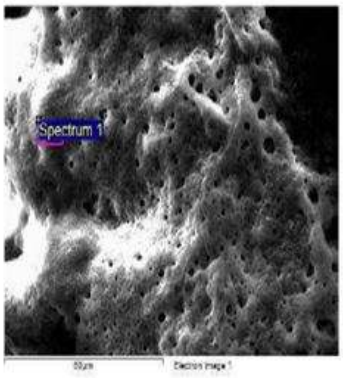

Figure 2a: EDX spectra of MgO:Dy^{3+} nanoparticles

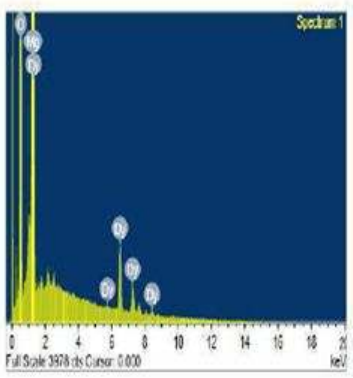

Figure 2b: EDX spectra of MgO:Dy^{3+}nanoparticles.

Field emission gun scanning electron microscope (FEGSEM)

Figure 3(a) shows the FEGSEM image of MgO:Dy^{3+} nanoparticles. The FEGSEM image is carried out by using Zeiss. Evo 18 Special Edition in order to analyse the structure and morphology of doped samples. SEM was used for the morphological study of MgO Doped with Dy. The instrument was accelerated at voltage of 10 Kv and the samples were scanned at a working distance of 8.5 mm.

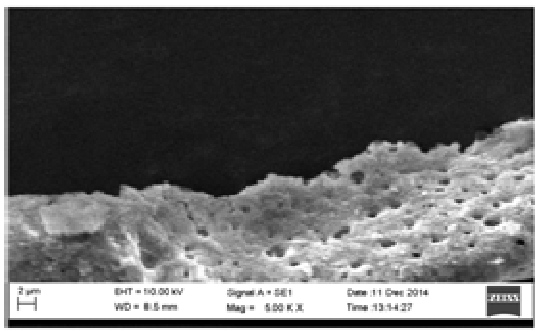

Figure 3(a): SEM image of MgO of different concentration of doped Dy^{3+} nanoparticles.

High resolution transmission electron microscope (HRTEM)

A typical HRTEM image of MgO:Dy^{3+} nanoparticles is shown in Fig.4 and Fig.5, respectively. The particle size obtained from HRTEM image is found to be in the range of 20 nm. HRTEM image clearly shows that the particles size is not spherical. The lattice fringes visible in the HRTEM micrograph are indicative of the crystalline nature of the particles. The three diffraction rings in the EDX patterns correspond to the (111), (200) and (220) reflections, confirming the cubic structure in accordance with XRD results.

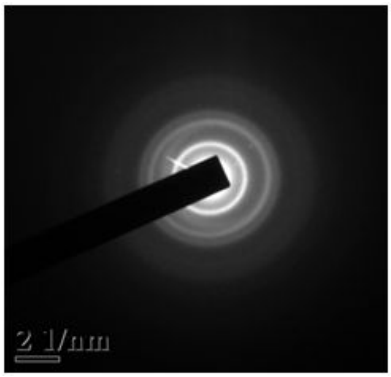

Figure 4. Selected Area Electron Diffraction (SAED) image of MgO:Dy^{3+} nanoparticles

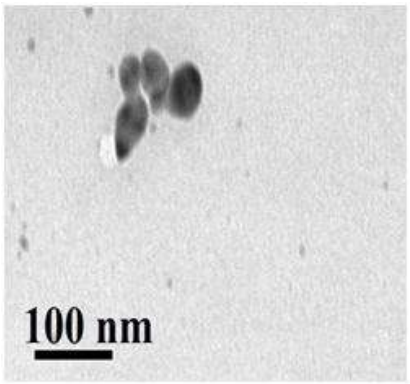

Figure 5 (a,) HRTEM image of MgO of different concentration of doped Dy^{3+} nanoparticles.

Fourier transforms infrared Spectra (FTIR)

Fig. 6 shows FTIR Spectra of MgO:Dy^{3+} particles are peaks at 3448 cm^{-1} and 2450 cm^{-1} corresponding to the O–H stretching mode of hydroxyl groups were present on the surface due to moisture. Peak at 1672 cm^{-1} was attributed to the bending vibration of water molecule. There are also small narrow bands at 1002 cm^{-1} which are due to the oxygen stretching and bending frequency. In

additions the bands at 1561 cm^{-1} and 1672 cm^{-1} are due to C-H stretching. The major peaks at 480 cm^{-1}, 678 cm^{-1} which confirmed the presence of Mg-O vibrations .

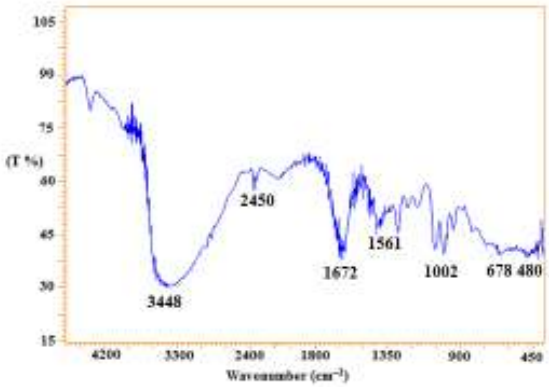

Figure 6: FTIR Spectra of MgO:Dy^{3+} nanoparticles

Thermoluminescence Study

Fig. 7 shows the recorded TL glow curve peak a,b,c,d of MgO:Dy^{3+} nanoparticles , exposed to UV-radiation, with different concentrations of Dy^{3+}.As could be seen in fig.7, the glow curve of MgO:$Dy^{3+,}$ exposed to UV-radiation , they have a simple structure with two prominent peak, one peak around 152 ^{0}C and second peak around 250 ^{0}C, moreover, the both peak does not shift towards to the shorter temperature, but intensity of glow peak increases with increasing dopant concentration of Dy^{3+} and was observe that (fig.7) the shape of the glow curve remains at almost the same for all the concentration of dopant. It is seen that the intensity of the peak of TL intensity increases with increasing concentration of the Dy^{3+}. Due to the increase in the concentration of Dy^{3+} the TL intensity also increases hence, it can be inferred that the peak intensity increases with increasing concentration of Dy^{3+} and the peak position does not shifts towards the lower temperature with the increasing concentration of Dy^{3+}.

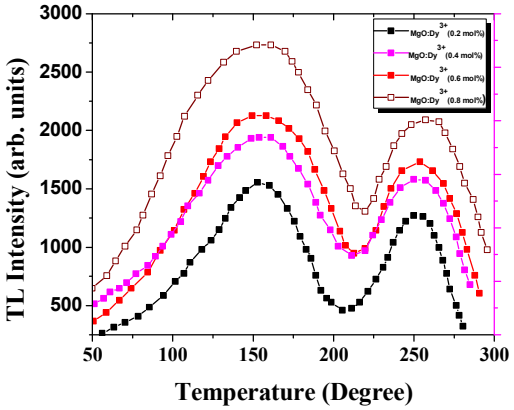

Figure 7: The TL glow curve of MgO:Dy^{3+} nanoparticles with different concentrations of Dy^{3+}

Glow Curve Convolution and De-convolution (GCCD)

To verify further, the energy levels of the glow peaks in UV-radiation irradiated sample of MgO:Dy^{3+} sample, their glow curves deconvolution was done (fig.8), using Glow Curve Deconvolution (GCD) functions suggested by [43] for first order, second, and general order glow curves, respectively. The functions are further modified for better accuracy. The modified formula were used for the deconvolution here (in fig.8) . The order of kinetics and activation energy of the isolated peak was found using Chen's set of empirical formulae [44,45], use of the correlation between order of kinetics and the form factor given by Chen was made. The frequency factor was obtained form the relation [44,45]. The concentration of Dy^{3+} the glow peak also increases with dopant. The activation energy of the samples was in the range for peak-I 0.46 eV to 0.42 eV and for peak-II 1.33 eV to .99 eV the order of frequency factor of the samples was found in the range for peak-I 1.01×10^{17} s^{-1} to 0.65×10^{16} s^{-1} and for peak-II 5.78×10^{28} s^{-1} and 2.78×10^{28} s^{-1} Table 4 shows The concentration of dopant, peak position, peak intensity of the MgO;Dy^{3+} nanoparticles and Table 5 shows The concentration of dopant, activation energy and frequency factor and order of kinetics of the MgO;Dy^{3+} nanoparticles . Fig.9 shows that the graph between the TL glow peak vs different concentrations of Dy^{3+}.

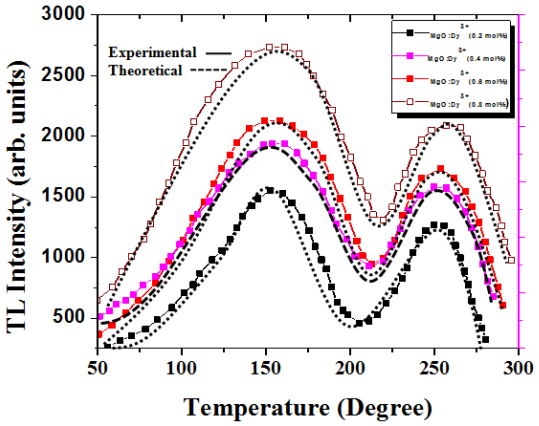

Figure 8: Comparison between the experimental (---) and and the theoretical (…) fitted glow curve of MgO:Dy^{3+} nanoparticles with UV-exposed.

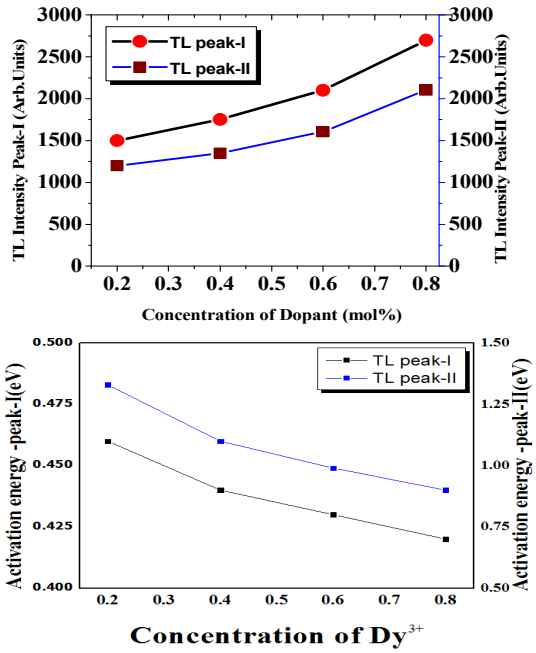

Figure 9: Graph between TL glow peak vs different concentrations of Dy^{3+} Figure.10 Graph between different concentrations of Dy^{3+} and activation energy.

CONCLUSION

The important conclusions drawn from the present study are as given below:

1. When the TL glow curve is recorded by heating the sample exposed to UV-radiation for 5 minutes, at a fixed heating rate 1^0 C/s, initially the TL intensity increases with temperature, attains a peak value I_m for a particular temperature, and then it decreases with further increase in temperature.
2. As the smaller particles have higher surface/volume ratio and more surface states, they contain more accessible carriers for TL. Furthermore, the carrier recombination rate increases with reducing size of the nanocrystals because of the increase of the overlap between electron and hole wave functions.
3. If the bottom of conduction band increases slowly with the reducing size of nanocrystals, and the energy level of trapping centre increase comparatively at higher rate with reducing size of crystals, then some decrease in the trap-depth can be obtained with reducing size of the nanoparticles and vice-versa. The equation for frequency factor is given by, $s = \frac{\beta E}{kT_m^2} exp\ (\frac{E}{KT_m})$. As E/T_m decreases with reducing size of nanoparticles, the frequency factor s decreases with reducing size of nanoparticles. It is to be noted that, although both E and T_m decrease with reducing size of nanoparticles, the ratio E/T_m decreases with reducing size of the nanoparticles because decrease of E with reducing size of nanoparticles is comparatively faster as compared to the decrease of T_m with reducing size of nanoparticles. As such the factor $exp\ (\frac{E}{KT_m})$ decreases with reducing size of nanoparticles. It is seen from Table1 that the shape factor determined from the equation, $\mu_g = \delta/\omega = (T_2-T_m)/(T_2-T_1)$, lies in the range from 0.51 to 0.40. Therefore, the TL follows second order kinetics because μ_g is nearly 0.42 [36].
4. The activation energy of the samples was in the range for peak-I 0.46 eV to 0.42 eV and for peak-II 1.33 eV to .90 eV the order of frequency factor of the samples was found in the range for peak-I 1.01×10^{17} s^{-1} to 0.65×10^{17} s^{-1} and for peak-II 5.78×10^{28} s^{-1} and 2.78×10^{28} s^{-1}

REFERENCES

McKeever SWS. Thermoluminescence of solids. UK: Cambridge University Press, 1988.

Furetta C. Handbook of thermoluminescence. Singapore: World Scientific Publishing Company Ltd, 2003.

Oberhofer M, Scharmann A. Applied thermoluminescence dosimetry. Cleveland, Ohio: CRC Press, 1981.

Vij DR. Luminescence of solids. New York: Plenum Press, 1998:361–89.

Fleming S.J. Thermoluminescence techniques in archaeology. Oxford: Clarendon Press, 1979.

Chandrakar R.K, Baghel R.N, Chandra B.P, Synthesis, characterization and thermoluminescence studies of Mn-doped ZnS nanoparticles, Luminescence, biological and chemical, 31(2015) 317-322.

Fendler J.H., Nanoparticles and Nanostructured Films Preparation, Characterization and Application, Wiley–VCH, Weinheim, 1994.

Trindade T., Brien P.O, Pickett N.L., Nanocrystalline Semiconductors: Synthesis, Properties, and Perspectives Chem.Mater., 2001;13;3843–3858.

Rao C.N.R., Kulkarni G.U., Thomas P.J., Edwards P.P., Size dependence chemistry : property of nanocrystals, Chem.Eur.J., 2002;8; 29–35.

Fatemeh Mohandes, Fatemeh Davar, Masoud Salavati-Niasari, Magnesium oxide nanocrystals via thermal decomposition of magnesium oxalate, Journal of Physics and Chemistry of Solids,2010;71;1623–1628.

Salavati-Niasari M., Fereshteh Z., Davar F., Magnesium oxide nanocrystals via thermal decomposition of magnesium oxalate Journal of Physics and Chemistry of Solids Volume, 2010,71, 1623–1628.

Ahniyaa,G.A., Seisenbaeva,L.H¨, aggstr¨om, Kamali S., Kessler V.G., Nordblad P, Johansson C., Bergstr¨om, Preparation of iron oxide nanocrystals by surfactant-free or oleic acid-assisted thermal decomposition of a Fe(III) alkoxide, J.Magn.Magn.Mater., 2008;320;781–787.

Wagner G.W., Bartram P.W., Koper O., Klabunde K.J., Reactions of VX, GD, and HD with Nanosize MgO, J.Phys.Chem.B, 1999;103; 3225–3228.

Liang S.H.C., Gay I.D., A ^{13}C solid-state NMR study of the chemisorption and decomposition of ethanol on MgO, J.Catal., 1986;101293–300.

Tsuji H., Yagi F., Hattori H., Kita H., Self-Condensation of n- Butyraldehyde over Solid Base Catalysts, J.Catal.,1994;148759–770.

YuanY.S., Wong M.S., Wong S.S., Solid-state processing and phase development of bulk $(MgO)_w$/BPSCCO high-temperature superconducting composite, J.Mater. Res.,1996;11;8–17.

Sterrer M., Diwald O., Knozinger E., Vacancies and Electron Deficient Surface Anions on the Surface of MgO Nanoparticles, J.Phys. Chem.B, 2000;104;3601–3607.

Fang H., Hu B., Wang L., Lu R., Yang C., Magnesium oxide nanocrystals via thermal decomposition of magnesium xalateront., Chem.China, 2008;3193– 197.

Ding Y., Zhang G., Wu H., Hai B. , Wang L., Qian Y., Chem.Mater. 2001;13;435–440.

Niu H., Yang Q., Tang K., Xie Y., Nanoscale Magnesium Hydroxide and Magnesium Oxide Powders: Control over Size, Shape, and Structure via Hydrothermal Synthesis, J.Nanoparticle Res.,2006;8;881–888.

El-Shall M., Slack W., Vann W., Kane D., Hanley D., Synthesis of Nanoscale Metal Oxide Particles Using Laser Vaporization/Condensation in a Diffusion Cloud Chamber, J.Phys.Chem., 1998; 98;3067–3070.

Matthews J.S., Just O., Obi-Johnson B., Rees W.S., CVD of MgO from a $Mg(\beta\text{-ketoiminate})_2$: Preparation, Characterization, and Utilization of an Intramolecularly Stabilized, Highly Volatile, Thermally Robust Precurso, Chem.VapourDeposition , 2000;6;129132-129140.

Bhargava A., Alarco J., Mackinnon I., Page D., Ilyushechkin A., Synthesis and characterisation of nanoscale magnesium oxide powders and their application in thick films of $Bi_2Sr_2CaCu_2O_8$, Mater.Lett.,1998;34;133–142.

Khairallah F., Glisenti A., Magnesium oxide nanocrystals via thermal decomposition of magnesium oxalate, J.Mol. Catal.Chem., 2007;274;137– 147.

Subramania A., G. Kumar V., Priya A.R.S., Vasudevan T., Polyol-mediated thermolysis process for the synthesis of MgO nanoparticles and nanowires

Nanotechnology, 2007;18 ; 225601–225605.

Makhluf S., Dror R., Nitzan Y., Abramovic Y., Jelinek H,R., Gedanken A., Microwave-Assisted Synthesis of Nanocrystalline MgO and Its Use as a Bacteriocide Adv.Funct., Mater., 2005;15;1708–1715.

Punfes V. F., Krishnan K. M., and Alivisatos A. P., Colloidal nanocrystal shape and size control: the case of cobalt, Science;2001; 291;245-250.

Xia Y., Yang P., Sun Y., Gate B., Yin Y., Kim F., and Yan H.. One diamensional nanostructural : synthesis characterization and application, Adv. Mater.,2003, 15, 353-359.

Salzemann C., Lisieki L., Brioude A., Urban J., and Pileni M. P., Collections of Copper Nanocrystals Characterized by Different Sizes and Shapes: Optical Response of These Nanoobjects, J. Phys. Chem.B, 2004; 108,13243-12250.

Choudhary V.R., Rane V.H., and Gadre R.V., Influence of Precursors Used in Preparation of MgO on Its Surface Properties and Catalytic Activity in Oxidative Coupling of Methane, J. Catal.,1994; 145, 300 -305.

SURESH S., ARIVUOLI D., Synthesis And Characterization of Pb+ Doped MgO Nanocrystalline Particles Digest , Journal of Nanomaterials and Biostructures, 2011;6,1597-1603.

Xu B.Q., Wei J.H., Wang H.Y., Sun K.Q., Zhu Q.M., Green Synthesis, Characterization and Application of MgO Nanoparticles using Rambutan Peel Extract, Cat.Today,2001; 68,217-220.

Utampanya S., Keabunde K.J., Schlup J.R., Nanoscale Metal Oxide Particles/Clusters as Chemical Reagents. Unique Surface Chemistry on Magnesium Oxide As Shown by Enhanced Adsorption of Acid Gases (Sulfur Dioxide and Carbon Dioxide) and Pressure Dependenc, Chem.Mater. 1991;3,175-180.

Roessler D.M., Walker W.C., Electronic Spectrum and Ultraviolet Optical Properties of Crystalline MgO, Phys. Rev., 1967; 159;733-738.

Klein C., Hurlbut C.S. Jr., Manual of Mineralogy, John Wiley & Sons, New York, 1999.

Sommerdijk J.L., Bril A., Efficiency of Dy^{3+}-Activated Phosphors, J. Electrochem. Soc.,1975; 122;952-958.

Sommerdijk J.L., Bril A., Efficiency of Dy^{3+}-Activated Phosphors, J. Electrochem. Soc.,1975; 122;952-958.

Xiao-Hua H., Feng-Yu G., Feng-Mei Z., Proceedings of the Third International Conference on Rare Earths,North-Holland, Amsterdam, 1979, 226-230.

Chen W, Wang Z, Lin Z, and Lin L., Thermoluminescence of ZnS nanoparticles,J. Appl. Phys. , 1997a82, 1465-1968.

Randall J. F and Wilkins M.H.F, Phosphorescence and electron traps. II. The interpretation of long-period phosphorescence; Proc. R.Soc., 1945a; 184; 366-370.

Randall J.F, and Wilkins M.H.F, Phosphorescence and electron traps. I. The study of trap distributions., Proc. R Soc.,1945b, 184, 390-395.

Efros Al. L. and. Efros A.L, Intraband absorption of light in semiconductor sphere., Sov. Phys. Semiconductors,1982;16;722-728.

Kitis Y, Ros J M, and Tuyn J.W.N, Thermoluminescence under an exponential heating function: II. Glow-curve deconvolution of experimental glow-curves, J.Phys.D:Appl.Phys. 31 (1998)2636.

Chen R, McKeever S.W.S, and Durrani S.A, Solution of the kinetic equations governing trap filling. Consequences concerning dose dependence and dose-rate effects, Phys. Rev. B, 24(1981)4931.

Kirsh Y., Kintic analysis of thermoluminescence, Phys.Stat.Sol., 129(1992)15-18.